

Data Release for CDMSlite Run 2 Period 1 LIP-search Analysis

SuperCDMS Collaboration

January 31, 2022

This document describes the public release of the data relevant to the SuperCDMS publication titled “Constraints on Lightly Ionizing Particles from CDMSlite” [1]. The upper limits on intensity of LIPs calculated using these data can be found in the associated paper [1]. Questions about the data or the limit calculations should be directed to supercdms_publications@lists.astro.caltech.edu.

1 Description of Files

1.1 Parameter Space

- *Mass_charge_bounds.txt*: This file contains the boundaries for mass vs charge parameter space for CDMSlite LIPs search analysis. LIPs have charge $q = \pm fe$, where e is the

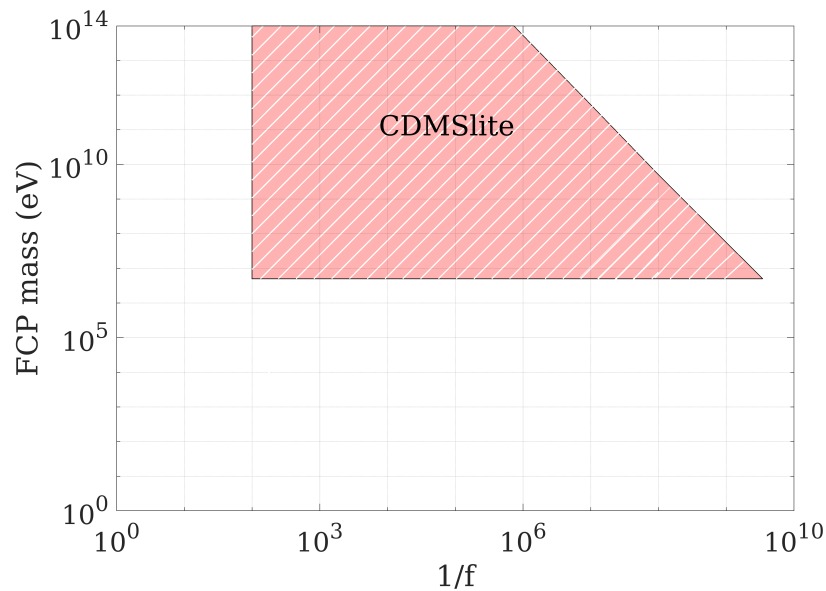


Figure 1: The mass vs charge parameter space for CDMSlite LIPs search analysis.

elementary charge and f has a value between 0 and 1. The first column consists of the

various f^{-1} values. The second and third columns consist of the lower mass bound and upper mass bound respectively. Figure 1 shows the mass versus charge parameter space of this analysis.

1.2 CDMSlite Run 2 Period 1 Data

- *EventEnergy_keVee.txt*: This file contains a column of event energies in units of keV_{ee} from CDMSlite Run 2 Period 1. The energy range used in the LIP-search results is 0.1 to 2 keV_{ee} ; the spectrum can be reproduced by using 190 bins of width 0.01 keV_{ee} with the lowest energy bin spanning 0.1–0.11 keV_{ee} . The file contains 180 events that pass all the selection criteria applied in the analysis. The spectrum generated is given in Fig. 2.

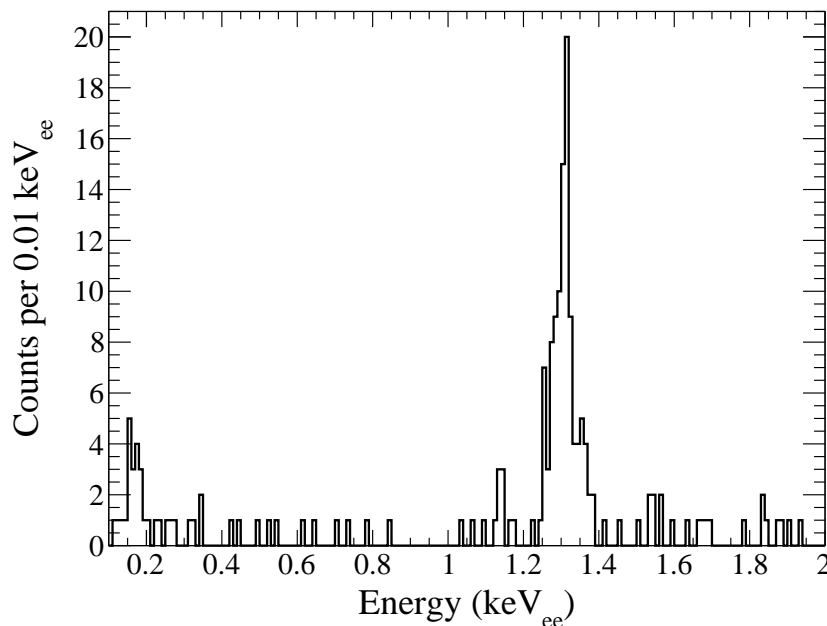


Figure 2: Energy spectrum of the CDMSlite Run2 Period1 data between 0.1 keV_{ee} and 2 keV_{ee} .

1.3 LIP Selection Efficiency

- *Efficiency_CDMSlite_Run2_Period1.txt*: This file contains LIP-selection efficiency, along with $\pm 1\sigma$ uncertainty, as a function of energies deposited in the detector for CDMSlite Run 2 Period 1. The data file has four columns; the description of each column is as follows.

Column 1: energies deposited in the detector,

Column 2: the efficiency at each energy,

Column 3: the 1σ lower bound for each efficiency value, and

Column 4: the 1σ upper bound for each efficiency value.

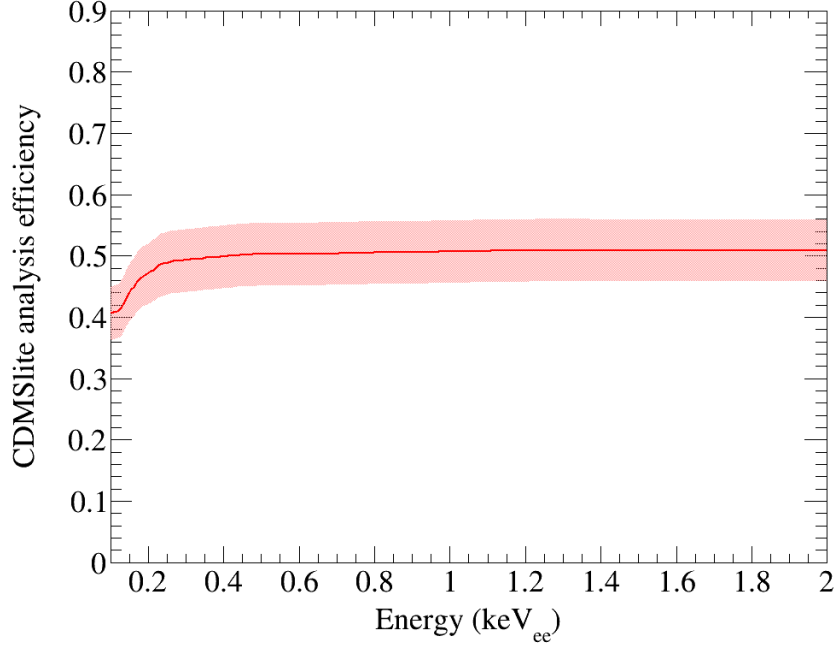


Figure 3: LIP selection efficiency along with $\pm 1\sigma$ uncertainty on the efficiency values for energy depositions between 0.1 keV_{ee} and 2 keV_{ee} .

Figure 3 shows the LIP signal efficiency as a function of energy in the range $0.1\text{--}2 \text{ keV}_{ee}$. The $\pm 1\sigma$ uncertainty band on the efficiency is also shown in the figure.

1.4 LIP Signal Model

- *CDMSlite_LIP_*_BetaGamma_@_#.txt*: The data to produce expected energy-deposition distributions for different charges and incident $\beta\gamma$ ¹ values is provided in these files. The energy-deposition distributions are calculated assuming isotropic or $\cos^2\theta$ angular distributions for LIPs incident on the CDMSlite detector. In the file-names, “*” refers to the f^{-1} values, “@” refers to the $\beta\gamma$ values and “#” refers to the angular distributions (isotropic and $\cos^2\theta$ distribution) of LIPs. Each data file has two columns: the first column is the energy deposition in eV and the second column is the probability density of energy deposition in the CDMSlite detector. The energy-deposition distributions are shown in Fig. 4.

1.5 LIP Efficiency Correction

- *LIPs_efficiency_correction.txt*: This file contains LIP-specific correction efficiency for various LIPs $\beta\gamma$ value. This efficiency is energy dependent and its value only depends on the LIP-charge, $\beta\gamma$ and assumed angular distribution. The uncertainty for all curves is smaller than 0.1%. The data file has seven columns; the description of each column is as follows:

¹ $\beta = v/c$ and $\gamma = 1/\sqrt{1 - \beta^2}$, where v is the LIP velocity.

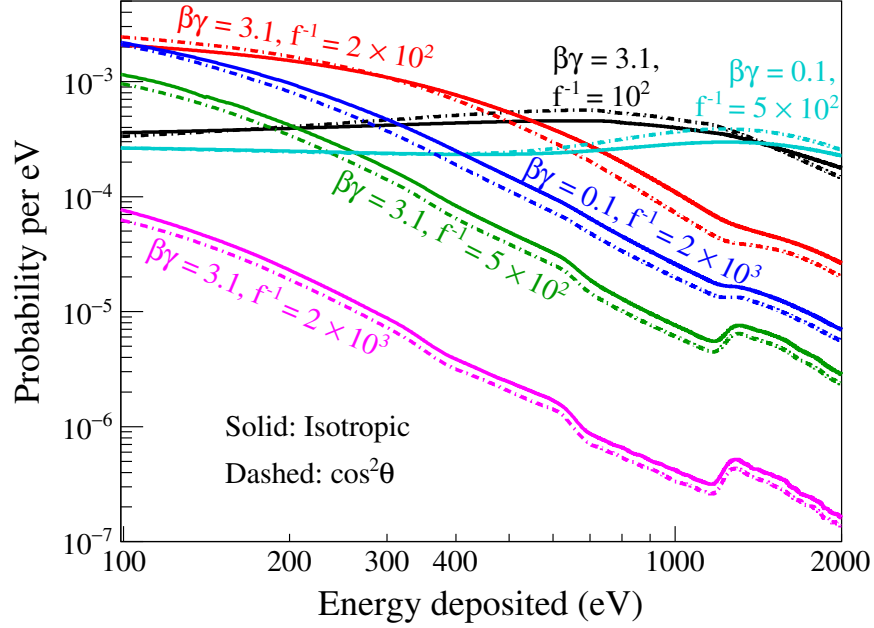


Figure 4: Simulated energy-deposition distributions averaged over incident angle for two different values of $\beta\gamma$ and various f^{-1} between 10^2 and 2×10^3 , after convolution with the detector energy resolution. The solid lines show the energy-deposition distributions assuming an isotropic incident LIP distribution, and the dash-dotted lines show the distribution assuming a $\cos^2 \theta$ incident distribution.

Column 1: various inverse LIPs charges (f^{-1}),

Column 2: LIPs efficiency correction factor for $\beta\gamma$ value 0.1 assuming cosine squared angular distribution,

Column 3: LIPs efficiency correction factor for $\beta\gamma$ value 0.1 assuming isotropic angular distribution,

Column 4: LIPs efficiency correction factor for $\beta\gamma$ value 0.3 assuming isotropic angular distribution,

Column 5: LIPs efficiency correction factor for $\beta\gamma$ value 1 assuming isotropic angular distribution,

Column 6: LIPs efficiency correction factor for $\beta\gamma$ value 3.1 assuming isotropic angular distribution, and

Column 7: LIPs efficiency correction factor for $\beta\gamma$ value 1000 assuming isotropic angular distribution.

Figure 5 shows the additional LIPs efficiency correction factors for various LIPs.

1.6 Intensity Limits

- *Intensity_figure_6.txt*: This file contains the limits on vertical intensity of LIPs for various LIPs $\beta\gamma$. The uncertainty band is only provided for $\beta\gamma = 0.1$ but is indicative of the size

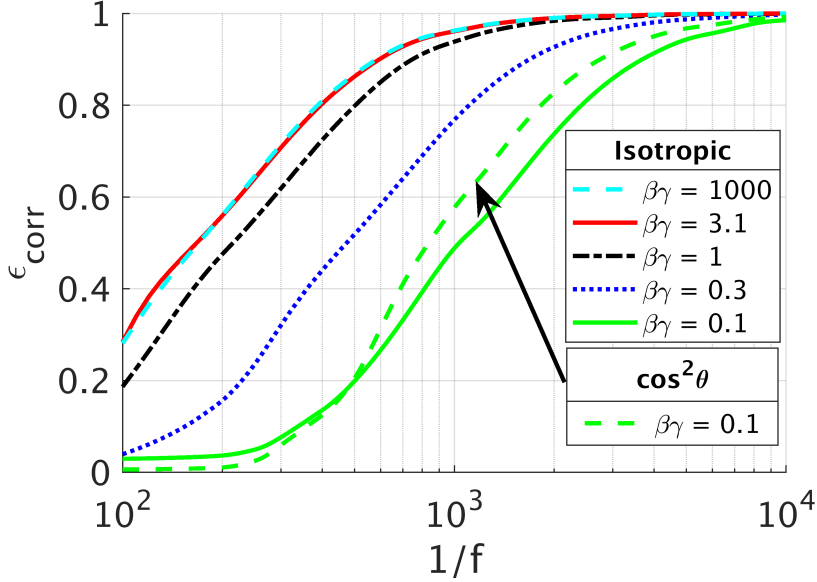


Figure 5: The LIP efficiency correction factor as a function of inverse LIP charge (f^{-1} for a variety of LIP $\beta\gamma$.

of the uncertainty of all the limit curves. The data file has nine columns; the description of each column is as follows:

Column 1: various inverse LIPs charges (f^{-1}),

Column 2: the 90% confidence limit on vertical intensity for LIPs with different f^{-1} for $\beta\gamma$ value 0.1 assuming an $\cos^2\theta$ distribution,

Column 3: the 90% confidence limit on vertical intensity for LIPs with different f^{-1} for $\beta\gamma$ value 1000 assuming an isotropic distribution,

Column 4: the 90% confidence limit on vertical intensity for LIPs with different f^{-1} for $\beta\gamma$ value 3.1 assuming an isotropic distribution,

Column 5: the 90% confidence limit on vertical intensity for LIPs with different f^{-1} for $\beta\gamma$ value 1.0 assuming an isotropic distribution,

Column 6: the 90% confidence limit on vertical intensity for LIPs with different f^{-1} for $\beta\gamma$ value 0.3 assuming an isotropic distribution,

Column 7: the 90% confidence limit on vertical intensity for LIPs with different f^{-1} for $\beta\gamma$ value 0.1 assuming an isotropic distribution,

Column 8: the lower limit of 1- σ uncertainty on the intensity limit for LIPs $\beta\gamma$ value 0.1 assuming isotropic distribution, and

Column 9: the upper limit of 1- σ uncertainty on the intensity limit for LIPs $\beta\gamma$ value 0.1 assuming isotropic distribution.

Figure 6 shows the 90 % confidence limit on LIP vertical intensity as a function of LIP electric charge for various values of LIP $\beta\gamma$.

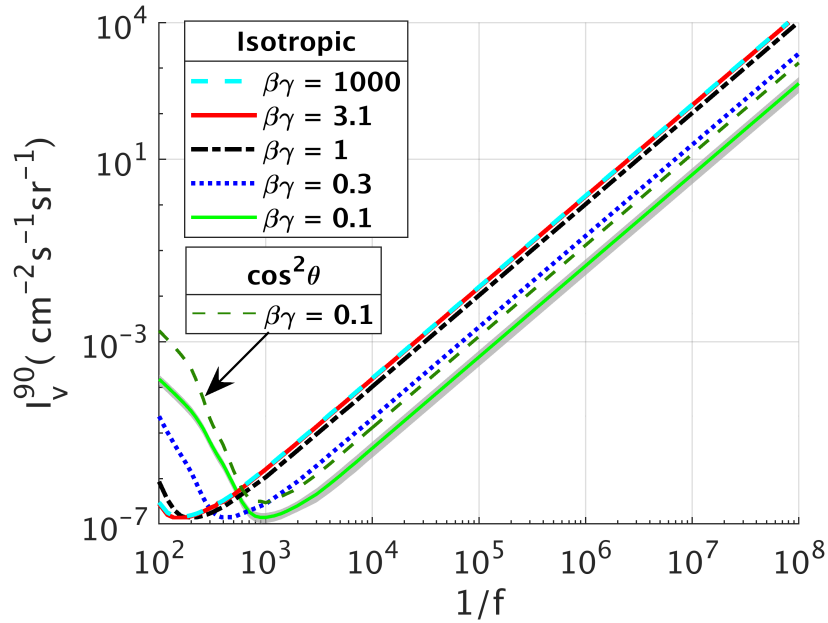


Figure 6: The 90 % confidence limit on LIP vertical intensity as a function of LIP electric charge for various values of LIP $\beta\gamma$. The limit curves for $\beta\gamma \geq 10^3$ coincide with each other and are represented by a single curve. For clarity, the uncertainty band (light green) is only shown for $\beta\gamma = 0.1$ but is indicative of the size of the uncertainty of all the limit curves.

References

- [1] I. Alkhatib et al. (SuperCDMS Collaboration), Phys. Rev. Lett. 127, 081802.